

# Targeted Synthesis of Two Super-Complex Zeolites with Embedded Isorecticular Structures

Jiho Shin,<sup>[a]</sup> Hongyi Xu,<sup>[b]</sup> Seungwan Seo,<sup>[a]</sup> Peng Guo,<sup>[b]</sup> Jung Gi Min,<sup>[a]</sup> Jung Cho,<sup>[a]</sup> Paul A. Wright,<sup>[c]</sup> Xiaodong Zou,<sup>\*[b]</sup> and Suk Bong Hong<sup>\*[a]</sup>

Dedication ((optional))

**Abstract:** We have recently proposed a novel structural coding approach that combines structure solution, prediction, and targeted synthesis of new zeolites with expanding complexity and embedded isorecticular structures. Two new zeolites in the RHO family, PST-20 and PST-25, were predicted and synthesized. Here, by extending this approach, we have predicted and synthesized for the first time the two next, higher generations of this family, PST-26 and PST-28, which have much larger unit cell volumes (422,655 Å<sup>3</sup> and 614,912 Å<sup>3</sup>, respectively) than those of the lower generations. We were able to confirm their crystallization by the combined use of powder X-ray and electron diffraction techniques. Aluminate and water contents in the synthesis mixture were found to be the two most critical factors influencing the structural expansion of embedded isorecticular zeolites under the synthesis conditions studied here.

Zeolites and molecular sieves continue to be widely used in a variety of commercial applications, including ion exchange, separation, and catalysis. The unique shape-selective properties of these microporous materials depend primarily on the size, shape, and/or dimensionality of their cavities and channels. As a result, much attention has been paid to the search for new types of zeolite structures over the last decades.<sup>[1-3]</sup> Although several millions of structures have been predicted upon developing more efficient computational and enumeration methods and algorithms,<sup>[4-6]</sup> the number of zeolite framework type codes approved by the Structure Commission of the International Zeolite Association remains only 230 or so.<sup>[7]</sup> Most of the zeolite structures synthesized directly in the laboratory have resulted from a conventional trial-and-error approach. This is also the case for the framework types derived from the rational synthetic strategies developed thus far. For example, the geometric correspondence between the organic structure-directing agents

(SDAs) encapsulated in the pores and the pore architecture of the resulting zeolite is generally loose, regardless of the size, shape, and rigidity of organic SDAs employed.<sup>[1-3]</sup> Although the introduction of heteroatoms like Ge into silicate frameworks can direct the formation of particular zeolite building units such as double 4-rings<sup>[8]</sup> and double 3-rings<sup>[9]</sup>, it is far from targeted synthesis of zeolites with designed structures.

Very recently, we have reported the crystal structure of zeolite ZSM-25 (framework type MWF),<sup>[10]</sup> which remained unsolved for more than 30 years. Our structure determination includes a combined use of single crystal three-dimensional electron diffraction data and phase information derived from the known structure of paulingite (PAU) which was found to have identical structural coding to ZSM-25. A similarity in the structures of zeolite Rho (RHO), paulingite, and ZSM-25 allowed us to discover a new principle of structure expansion (Figure 1) and thus to define them as the RHO family of zeolites with embedded isorecticular structures. The structural expansion principle in the RHO family is substantially different from that normally found in metal-organic frameworks<sup>[11,12]</sup> in that the space between the scaffolds is filled by four other cage types to form a fully tetrahedrally-coordinated framework, giving each of its members different framework topologies but the same maximum ring size.

We were also able to predict the two higher generations of the RHO family of increasingly complex zeolites, denoted RHO-G5 and RHO-G6, and then to synthesize them via a rational approach, denoted PST-20 and PST-25, respectively.<sup>[10]</sup> The structure prediction was based on the strong reflections approach, i.e., similar distribution of diffraction intensities in reciprocal space of the zeolites in the RHO family. In this communication we report the prediction of the next two even more super-complex generations (RHO-G7 and RHO-G8; Supporting Information, Figure S1) of the RHO family based on a new and simpler approach compared to the strong reflections approach used in our recent work.<sup>[10]</sup> We also show that they can be synthesized by varying the concentrations of inorganic components in the synthesis mixture yielding PST-20. The formation of these targeted materials has been confirmed not only by the LeBail refinement of the synchrotron powder X-ray diffraction (XRD) patterns of crystallized products, but also by selected area electron diffraction (SAED) patterns from which the structural information on the scaffold expansion along each unit-cell edge and the manner of inter-scaffold space filling in the RHO family of zeolites can be directly obtained.

The scaffold of the RHO family, which constitutes [4<sup>12</sup>6<sup>8</sup>8<sup>6</sup>] (*Ita*), [4<sup>8</sup>8<sup>2</sup>] (*d8r*), and [4<sup>12</sup>8<sup>6</sup>] (*pau*) cages, can be expanded by continuously adding an extra pair of *pau* and *d8r* cages along each unit-cell edge, as noted in our recent work.<sup>[10]</sup> Although the

[a] Dr. J. Shin,<sup>[§]</sup> S. Seo, J. G. Min, J. Cho, Prof. S. B. Hong  
Center for Ordered Nanoporous Materials Synthesis,  
School of Environmental Science and Engineering, POSTECH,  
Pohang 790-784, Korea  
E-mail: sbhong@postech.ac.kr

[b] Dr. H. Xu,<sup>[§]</sup> P. Guo, Prof. X. Zou  
Inorganic and Structural Chemistry and Berzellii Center EXSELENT  
on Porous Materials, Department of Materials and Environmental  
Chemistry, Stockholm University, SE-106 91 Stockholm, Sweden  
E-mail: xzou@mmk.su.se

[c] Prof. P. A. Wright  
EaStCHEM School of Chemistry, University of St. Andrews, St.  
Andrews, Fife KY16 9ST, UK

[§] Present address: Inorganic and Structural Chemistry and Berzellii  
Center EXSELENT on Porous Materials, Department of Materials  
and Environmental Chemistry, Stockholm University, SE-106 91  
Stockholm, Sweden

[+] These authors contributed equally to this work.

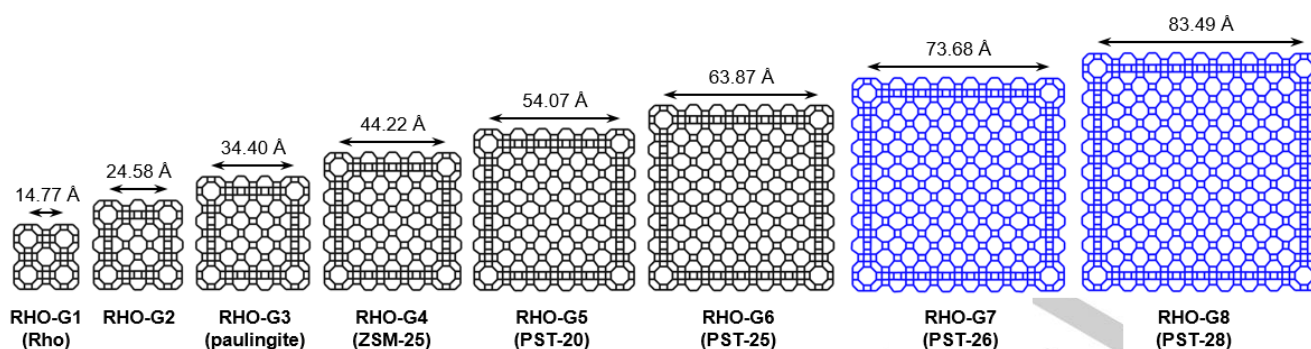


**Figure 1.** Framework representations of cross-sections (ca. 12 Å thick) of RHO-G1 to RHO-G8 in the RHO-family of zeolites. The two structures furthest right have been predicted and then synthesized in this work.

**Table 1.** Syntheses from gel composition 5.2R-1.9Na<sub>2</sub>O-0.5Ca(NO<sub>3</sub>)<sub>2</sub>-xAl<sub>2</sub>O<sub>3</sub>-7.2SiO<sub>2</sub>-yH<sub>2</sub>O.<sup>[a]</sup>

Run	Gel composition		Product <sup>[b]</sup>
	SiO <sub>2</sub> /Al <sub>2</sub> O <sub>3</sub>	H <sub>2</sub> O/SiO <sub>2</sub>	
1	7.2	54.2	PST-20 + ZSM-25 + gismondine
2	7.2	41.7	PST-25 + PST-20 + gismondine
3	7.2	34.7	PST-26 + PST-25 + gismondine
4	7.2	27.8	gismondine + (PST-26) + (PST-25)
5	4.8	34.7	gismondine
6	4.8	27.8	gismondine
7	9.6	34.7	PST-25 + PST-26 + PST-20
8	9.6	27.8	PST-26 + PST-28 + PST-25
9	9.6	20.8	PST-26 + PST-28 + PST-25 + mordenite
10	14.4	34.7	mordenite + PST-25 + PST-20
11	14.4	27.8	mordenite + (PST-26) + (PST-25)

[a] R is tetraethylammonium bromide, and x and y are varied between 0.5 ≤ x ≤ 1.5 and 150 ≤ y ≤ 390, respectively. The final synthesis mixture was stirred at 80 °C for 24 h, and crystallization was performed under rotation (60 rpm) at 145 °C for 2 days. [b] The phase appearing first is the major phase, and the product obtained in a trace amount is given in parentheses.

strong reflections approach in reciprocal space can be applied to predict higher generations of the RHO family, the procedures get more complex with the increasing number of symmetry-independent atoms to be located in the electron density maps.

Here we have developed a new and more convenient model building approach based on the structural coding in real space. Since both set of scaffold and embedded cages in this family are repetitive, the appropriate structure fragments of RHO-G7 and RHO-G8 were predicted from their lower generations, i.e., RHO-G6 (PST-25) and RHO-G7, respectively. The detailed prediction procedures can be found in Supporting Information. The asymmetric units of RHO-G7 and RHO-G8 possess 72 and 104 topologically distinct tetrahedral atoms, together with 168 and 240 such O atoms (Supporting Information, Tables S1-S3). When inspecting the evolution of cage types within members of the RHO family, we found that the numbers of three embedded cages, i.e., [4<sup>6</sup>8<sup>4</sup>] (*t-gsm*), [4<sup>5</sup>8<sup>3</sup>] (*t-oto*), and [4<sup>7</sup>8<sup>5</sup>] (*t-phi*) cages, increase much more rapidly than those of the other cage types (*lta*, *d8r*, *pau*, and [4<sup>6</sup>6<sup>2</sup>8<sup>6</sup>] (*t-plg*)) as the members become more complex. For example, ZSM-25 consists of 60 *t-gsm*, 144 *t-oto* and 72 *t-phi* cages per unit cell, whereas RHO-G5 and RHO-G6 constitute 168 and 360 *t-gsm*, 240 and 360 *t-oto*, and 144 and 240 *t-phi* cages per unit cell, respectively, so that RHO-G7 and RHO-G8 constitute 660 and 1092 *t-gsm*, 504 and 672 *t-oto*, and 360 and 504 *t-phi* cages per unit cell, respectively (Supporting Information, Table S4). Also, their unit cell volumes were calculated as 422,655 Å<sup>3</sup> and 614,912 Å<sup>3</sup>, which are

respectively ca. 1.5 and 2.2 times larger than the volume (275,132 Å<sup>3</sup>) of PST-25, the largest zeolite structure known to date. The simulated powder XRD patterns of RHO-G7 and RHO-G8 are given in Supporting Information Figure S2.

Previously, the rapid increase of the numbers of *t-gsm*, *t-oto*, and *t-phi* cages with the increased generations of the RHO family inspired us to search for zeolites that contain those cages. We found that natural zeolites gismondine (GIS) contains only *t-gsm* cages, while the phillipsite (PHI) contains *t-oto* and *t-phi* cages as building units. They are reported to possess substantial amounts of Ca<sup>2+</sup> and even Ba<sup>2+</sup> as extraframework cations.<sup>[13,14]</sup> To promote the crystallization of higher generations of the RHO family, therefore, we introduced a small amount of alkaline-earth cations, especially Ca<sup>2+</sup> and Sr<sup>2+</sup>, to the ZSM-25 synthesis mixture. This rational approach finally allowed us to synthesize the two resulting super-complex zeolites, PST-20 (RHO-G5) and PST-25 (RHO-G6), respectively.<sup>[10]</sup>

The tetraethylammonium (TEA<sup>+</sup>)-mediated syntheses of the RHO family of zeolites (i.e., ECR-18 (RHO-G3), ZSM-25 (RHO-G4), PST-20 (RHO-G5), and PST-25 (RHO-G6)) reported thus far reveal that the phase selectivity of the crystallization differs notably according to the SiO<sub>2</sub>/Al<sub>2</sub>O<sub>3</sub> and H<sub>2</sub>O/SiO<sub>2</sub> ratios in the synthesis mixture, as well as to the type of inorganic cations employed.<sup>[10,15-17]</sup> Thus, our initial attempts to synthesize the predicted RHO-G7 and RHO-G8 varied the water and aluminate contents in the synthesis mixture. Table 1 lists the representative products from syntheses in the mixed TEA<sup>+</sup>-Na<sup>+</sup>-Ca<sup>2+</sup> SDA system and aluminosilicate gels in which the SiO<sub>2</sub>/Al<sub>2</sub>O<sub>3</sub> and H<sub>2</sub>O/SiO<sub>2</sub> ratio are in the ranges 4.8 - 14.4 and 20.8 - 54.2, respectively. The phase selectivity of the crystallization is very sensitive to both SiO<sub>2</sub>/Al<sub>2</sub>O<sub>3</sub> and H<sub>2</sub>O/SiO<sub>2</sub> ratios in the gel. When the initial SiO<sub>2</sub>/Al<sub>2</sub>O<sub>3</sub> ratio in the gel was fixed to 7.2, for example, a decrease in H<sub>2</sub>O/SiO<sub>2</sub> ratio resulted in the formation of increasingly more complex generations of the RHO family. However, unlike ZSM-25 and PST-20,<sup>[10,16]</sup> the lower generations of this family of embedded isorecticular zeolites, we could only obtain them as their mixtures, together with a small amount of gismondine (Table 1). A plausible explanation for this will be given below.

When using an aluminosilicate gel with H<sub>2</sub>O/SiO<sub>2</sub> = 34.7, we were able to find signs of the crystallization of RHO-G7, denoted PST-26. This suggests that a decrease in H<sub>2</sub>O/SiO<sub>2</sub> ratio leads to the preferential formation of *t-oto*, *t-gsm*, and *t-phi* cages over that of the other four types of cages (i.e., *lta*, *d8r*, *pau*, and *t-plg*

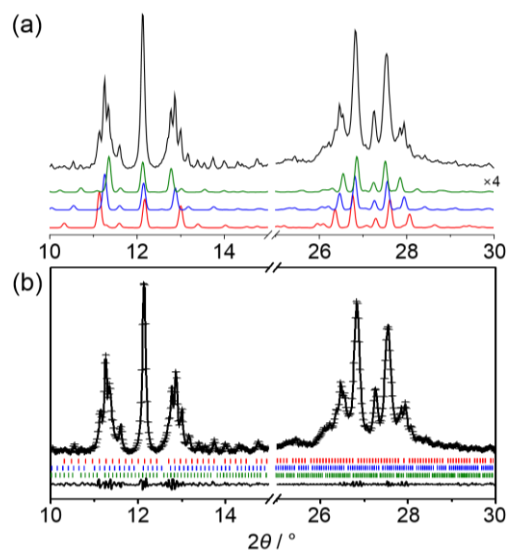


**Figure 2.** (a) Synchrotron powder XRD pattern of the solid product obtained from run 8 in Table 1: experimental (top trace), simulated (bottom three traces). The simulated patterns of RHO-G6, RHO-G7, and RHO-G8 are given from bottom to top, respectively ( $\lambda = 1.4865 \text{ \AA}$ ). The intensity of the simulated PXRD patterns in the region of  $25 - 30^\circ$  was multiplied by 4. (b) Three-phase (PST-25, PST-26, and PST-28) LeBail fit for the same product: observed data (crosses), calculated fit (solid line) and difference plot (lower trace). Red, blue, and green vertical bars indicate the positions of Bragg peaks of PST-25, PST-26, and PST-28, respectively.

cages), thus favoring the formation of more complex higher generations. However, a further decrease in  $\text{H}_2\text{O}/\text{SiO}_2$  ratio to 27.8 in the gel yielded gismondine together with trace amounts of PST-25 and PST-26. Therefore, we carried out syntheses using aluminosilicate gels of varying Si/Al ratios while keeping their  $\text{H}_2\text{O}/\text{SiO}_2$  ratio to 34.7 or lower. Gismondine crystallized from synthesis mixtures with  $\text{SiO}_2/\text{Al}_2\text{O}_3 = 4.8$  and  $\text{H}_2\text{O}/\text{SiO}_2 \leq 34.7$ . As shown in Table 1, synthesis using a gel with  $\text{SiO}_2/\text{Al}_2\text{O}_3 = 9.6$  and  $\text{H}_2\text{O}/\text{SiO}_2 = 27.8$  gave a product containing RHO-G8 (PST-28), the next super-complex generation of the RHO family. When the  $\text{H}_2\text{O}/\text{SiO}_2$  ratio in the synthesis mixture was decreased further to 20.8 under the conditions mentioned above, mordenite (MOR) began to appear. Further increase in  $\text{SiO}_2/\text{Al}_2\text{O}_3$  ratio to 14.4 yielded a mixture of mordenite and the RHO family of zeolites.

Figure 2 shows the selected regions ( $2\theta = 10 - 15^\circ$  and  $25 - 30^\circ$ ) of the synchrotron powder XRD pattern of the product obtained from run 8 in Table 1. Included for comparison are the simulated XRD patterns of hypothetical zeolite structures RHO-G6, RHO-G7, and RHO-G8. It can be seen that this product is a mixture of RHO-G6 (PST-25, ca. 20%), RHO-G7 (PST-26, ca. 45%), and RHO-G8 (PST-28, ca. 35%) (Supporting Information Figure S3). As shown in Figure 2 and Supporting Information Figure S4, the three-phase LeBail refinement based on PST-25, PST-26, and PST-28 provides a good agreement between the observed and calculated profiles ( $R_{\text{wp}} = 0.0190$ ,  $R_{\text{p}} = 0.0131$ ). The lattice parameters obtained were  $a = 65.03969(6) \text{ \AA}$  for PST-25,  $a = 75.0462(5) \text{ \AA}$  for PST-26, and  $a = 85.0363(5) \text{ \AA}$  for PST-28.

It is also remarkable that the  $\text{Na}^+$ -exchanged form of the

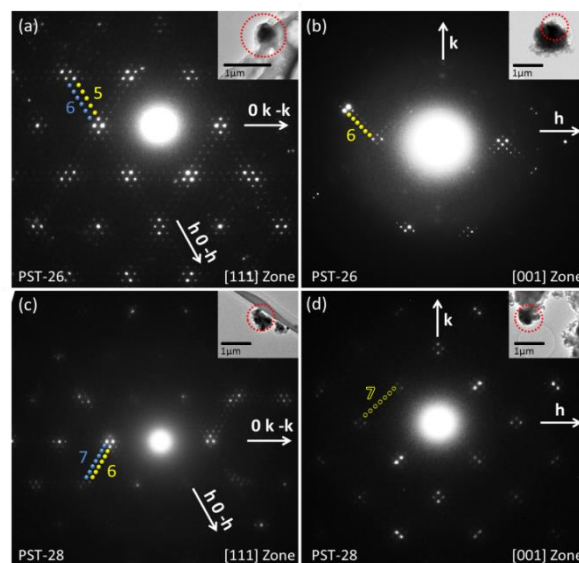


**Figure 3.** SAED patterns of PST-26 (a and b) and PST-28 (c and d) along the [111] and [001] zone axes, respectively. The number of weak diffraction spots is marked to illustrate the distinguishable structural features of both zeolites. Since the weak diffraction spots in (d) are not observable, the distance between two closest strong spots are used to predict the expected position of weak spots.

product from run 8 is characterized by a  $\text{CO}_2$  uptake of  $2.6 \text{ mmol g}^{-1}$  at  $1.0 \text{ bar}$  and  $25^\circ \text{C}$ , which is somewhat lower than the uptakes ( $\leq 3.2 \text{ mmol g}^{-1}$ ) of the lower, pure generations of the RHO family of zeolites such as ZSM-25 and Na-PST-20.<sup>[10]</sup> (Supporting Information Figure S5). Because this product, as well as the product (i.e., a physical mixture of PST-25, PST-26, and PST-20) obtained from run 7, loses the crystallinity after calcination under flowing air at  $550^\circ \text{C}$  for 6 h, like PST-20, the higher generation of this family may in our view have poorer structural stability than the lower one. If such is the case, this would then rationalize the relatively low  $\text{CO}_2$  uptake of the product from run 8.

Figure 3 shows the SAED patterns of PST-26 and PST-28 crystals in the product described above, taken along both [111] and [001] zone axes. As recently reported,<sup>[10]</sup> the intensity distributions of reflections observed in the SAED patterns of these materials are similar to each other due to close resemblance in the manner of the scaffold expansion and inter-scaffold space filling. The SAED patterns of PST-26 are characterized by the relation  $d_{(10-1)} = d_{(-110)} = d_{(110)} = 52.71(5) \text{ \AA}$ , implying that  $a = 74.53(9) \text{ \AA}$ . Similarly, those of PST-28 show that  $d_{(10-1)} = d_{(-110)} = d_{(110)} = 60.60(6) \text{ \AA}$  and thus  $a = 85.69(7) \text{ \AA}$ . The fact these lattice parameters are in excellent agreement with the powder XRD results confirms the successful crystallization of both of the predicted phases RHO-G7 (PST-26) and RHO-G8 (PST-28).

Another important result obtained from Figure 3 is that the number of weak reflections between the strong reflections differs systematically according to the generation number of the members of the RHO family. In the SAED patterns of ZSM-25 and PST-20 taken along the [111] zone axis, for example, there are two/three and three/four weak reflections between two



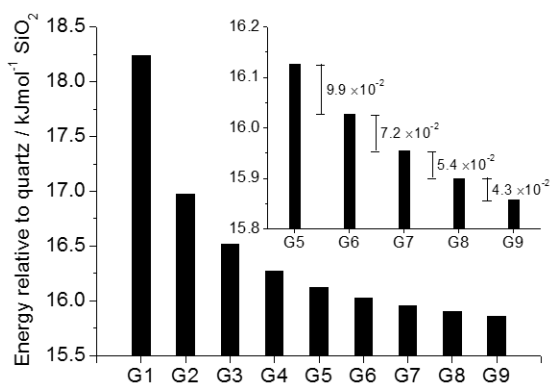


**Figure 4.** Lattice energies relative to quartz of the RHO-*Gn* structures in the RHO family calculated by GULP.<sup>[16]</sup> The relative energies corresponding to higher generation structures are magnified to more precisely show their gradual decrease.

strong reflections, respectively (Supporting Information, Figure S6). Moreover, four/five, five/six, and six/seven weak reflections are observable between each pair of strong reflections in the patterns of PST-25, PST-26, and PST-28, respectively. This trend of the increasing number of weak reflections between the strong reflections also holds for the SAED patterns taken along the *c*-axis.

Despite the considerable synthetic efforts, none of our attempts to crystallize PST-25, PST-26, and PST-28 as their pure form has yet been successful, in contrast to the case of ZSM-25 and PST-20.<sup>[10,16]</sup> We think that this may be attributed to the similarity in their thermodynamic stabilities. As shown in Figure 4, in fact, the energy difference between two adjacent generations, calculated using the program GULP,<sup>[18]</sup> becomes gradually smaller as the generation number (*n*) of the members (RHO-*Gn*'s) of the RHO family of zeolites increases. Therefore, it appears to become more difficult to obtain the pure form of higher generation members with increasing the generation number at least in the mixed TEA<sup>+</sup>-Na<sup>+</sup>-Ca<sup>2+</sup> (or the other alkaline earth cations) SDA system. In our view, a similar trend may also be observed for other families of zeolites with embedded isorecticular structures, especially when their members are synthesized in similar SDA systems.

In summary, we have first predicted and then successfully synthesized two more-complex, higher generations in the RHO family of zeolites, denoted PST-26 and PST-28, respectively. The overall results of this work, as well as those of our recent study,<sup>[10]</sup> demonstrate that the type and concentration of inorganic cations and the aluminate and water contents in synthesis mixtures containing TEA<sup>+</sup> ions as an organic SDA are critical factors affecting the structural complexity of embedded isorecticular zeolites crystallized. We anticipate that our structural coding concept will further be used to achieve "fully rational" synthesis of zeolites with designed structures and properties.

## Acknowledgements

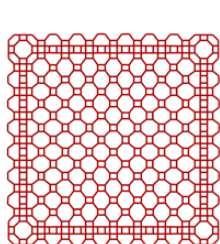
This work was supported by the NCRI (2012R1A3A-2048833) and BK 21-plus programs through the National Research Foundation of Korea, the Swedish Research Council (VR), the Swedish Governmental Agency for Innovation Systems (VINNOVA), the Röntgen-Ångström Cluster through the project grant MATsynCELL, and the Knut and Alice Wallenberg Foundation through the project grant 3DEM-NATUR. We thank PAL (Pohang, Korea) for synchrotron diffraction beam time. PAL is supported by MSIP and POSTECH.

**Keywords:** embedded isorecticular structures • RHO family • structure prediction • synthesis design • zeolites

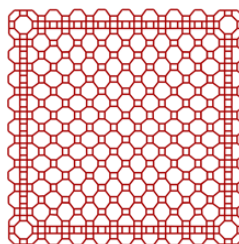
- [1] a) M. A. Cambor, S. B. Hong, In *Porous Materials*; b) D. W. Bruce, D. O'Hare, R. I. Walton, Eds.; Wiley: Chichester, **2011**, pp. 265-325.
- [2] M. Moliner, F. Rey, A. Corma, *Angew. Chem. Int. Ed.* **2013**, *52*, 13880-13889; *Angew. Chem.* **2013**, *125*, 14124-14134.
- [3] M. Moliner, C. Martinez, A. Corma, *Angew. Chem. Int. Ed.* **2015**, *54*, 3560-3579; *Angew. Chem.* **2015**, *127*, 3630-3649.
- [4] M. M. J. Treacy, I. Rivin, E. Balkovsky, K. H. Randall, M. D. Foster, *Microporous Mesoporous Mater.* **2004**, *74*, 121-132.
- [5] R. Pophale, P. A. Cheeseman, M. W. Deem, *Phys. Chem. Chem. Phys.* **2011**, *13*, 12407-12412.
- [6] a) J. V. Smith, *Chem. Rev.* **1988**, *88*, 149-182; b) M. O'Keeffe; S. T. Z. Hyde, *Z. Kristallogr.* **1996**, *211*, 73-78; c) O. D. Friedrichs, A. W. M. Dress, D. H. Huson, J. Klinowski, A. L. Mackay, *Nature*, **1999**, *400*, 644-647; d) M. D. Foster, M. M. J. Treacy, J. B. Higgins, I. Rivin, E. Balkovsky, K. H. Randall, *J. Appl. Cryst.* **2005**, *38*, 1208-1030.
- [7] International Zeolite Association, Structure Commission, <http://www.iza-structure.org>.
- [8] L. Tang, L. Shi, C. Bonneau, J. L. Sun, H. J. Yue, A. Ojuva, B. L. Lee, M. Kritikos, R. G. Bell, Z. Bacsik, J. Mink, X. D. Zou, *Nat. Mater.* **2008**, *7*, 381-385.
- [9] Y. Yun, M. Hernández, W. Wan, X. Zou, J. L. Jordá, A. Cantin, F. Rey, A. Corma, *Chem. Commun.* **2015**, *51*, 7602-7605.
- [10] P. Guo, J. Shin, A. G. Greenaway, J. G. Min, J. Su, H. J. Choi, L. Liu, P. A. Cox, S. B. Hong, P. A. Wright, X. Zou, *Nature* **2015**, *524*, 74-78.
- [11] M. Eddaoudi, J. Kim, N. Rosi, D. Vodak, J. Wachter, M. O'Keeffe, O. M. Yaghi, *Science* **2002**, *295*, 469-472.
- [12] H. Deng, S. Grunder, K. E. Cordova, C. Valente, H. Furukawa, M. Hmadeh, F. Gándara, A. C. Whalley, Z. Liu, S. Asahina, H. Kazumori, M. O'Keeffe, O. Terasaki, J. F. Stoddart, O. M. Yaghi, *Science* **2012**, *336*, 1018-1023.
- [13] K. Fischer, V. Schramm, *Adv. Chem. Ser.* **1971**, *101*, 250-258.
- [14] R. Rinaldi, J. J. Pluth, J. V. Smith, *Acta Crystallogr.* **1974**, *B30*, 2426-2433.
- [15] D. E. W. Vaughan, K. G. Strohmaier, *Microporous Mesoporous Mater.* **1999**, *28*, 233-239.
- [16] S. B. Hong, W. C. Paik, W. M. Lee, S. P. Kwon, C.-H. Shin, I.-S. Nam, B.-H. Ha, *Stud. Surf. Sci. Catal.* **2001**, *135*, 186-193.
- [17] D. J. Kim, C.-H. Shin, S. B. Hong, *Microporous Mesoporous Mater.* **2005**, *83*, 319-325.
- [18] J. D. Gale, A. L. Rhol, *Mol. Simul.* **2003**, *29*, 291-341.

## COMMUNICATION

Targeted synthesis of two more-complex, higher generations in the RHO family of zeolites with embedded isorecticular structures, PST-26 and PST-28 is presented.



RHO-G7 (PST-26)



RHO-G8 (PST-28)

Jiho Shin, Hongyi Xu, Seungwan Seo, Peng Guo, Jung Gi Min, Jung Cho, Paul A. Wright, Xiaodong Zou,\* and Suk Bong Hong\*

Page No. – Page No.

**Targeted Synthesis of Two Super-Complex Zeolites with Embedded Isorecticular Structures**

WILEY-VCH